

General scatterings and electronic states in the quantum-wire network of moiré systems

Chen-Hsuan Hsu^{1,2,3}, Daniel Loss^{3,4}, and Jelena Klinovaja⁴

¹*Yukawa Institute for Theoretical Physics, Kyoto University, Kyoto 606-8502, Japan*

²*Institute of Physics, Academia Sinica, Taipei 115, Taiwan*

³*RIKEN Center for Emergent Matter Science, Wako, Saitama 351-0198, Japan*

⁴*Department of Physics, University of Basel, Klingelbergstrasse 82, CH-4056 Basel, Switzerland*

(Dated: September 4, 2023)

We investigate electronic states in a two-dimensional network consisting of interacting quantum wires, a model adopted for twisted bilayer systems. We construct general operators which describe various scattering processes in the system. In a twisted bilayer structure, the moiré periodicity allows for generalized umklapp scatterings, leading to a class of correlated states at certain fractional fillings. We identify scattering processes which can lead to an insulating gapped bulk with gapless chiral edge modes at fractional fillings, resembling the quantum anomalous Hall effect recently observed in twisted bilayer graphene. Finally, we demonstrate that the description can be useful in predicting spectroscopic and transport features to detect and characterize the chiral edge modes in the moiré-induced correlated states.

Moiré bilayer structures provide a platform for strongly correlated systems, where unconventional states of matter emerge [1–4] as a consequence of flat energy bands [5]. Since the discovery of correlated insulating states and superconductivity in twisted bilayer graphene (TBG) [6, 7], various exotic states or features have been observed [8], including nematicity [9–12], pressure-enhanced superconductivity [13], strange metal [14, 15], cascade of transitions [16, 17], orbital magnetism [18, 19], independent superconducting and correlated insulating states [20–22], fragile correlated states against twist angle disorder [23], entropy-driven phase transition [24, 25], unconventional superconductivity [26], and spin-orbit-driven ferromagnetism [27].

In addition to features that resemble existing strongly correlated systems such as cuprates and iron-based superconductors, there are observations suggesting the existence of topological phases. Specifically, nonlocal transport demonstrated the presence of chiral edge modes at 3/4 filling in TBG [28], accompanied by the quantization of Hall resistance at zero magnetic fields [29]. More recent studies revealed a series of quantum anomalous Hall or Chern insulators with Chern numbers $C = \pm 1, \pm 2$ and ± 3 at $\pm 3/4, \pm 1/2$ and $\pm 1/4$ fillings, respectively [30–32]. Furthermore, there is experimental indication of a many-body origin for the topological phases [27, 30–36]. The observations on various electronic states motivated theoretical studies on TBG [37–53] and the development of moiré electronics, including structures beyond bilayers [54–63] and materials other than graphene [64–69].

A major theoretical challenge in strongly correlated moiré systems involves incorporating many-body effects with numerous atoms due to the large moiré unit cell. It is thus crucial to identify the relevant degrees of freedom to construct an effective model for efficient quantitative analysis. Remarkably, correlated phenomena in TBG can be investigated in the context of (Tomonaga-)Luttinger liquids, which inherently includes electron-electron interactions [70–72]. Specifically, in the presence of an interlayer potential difference, one-dimensional channels emerge at domain walls between

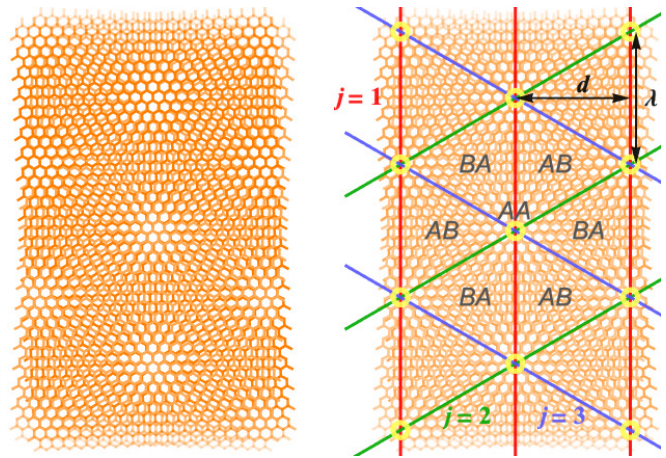


FIG. 1. Moiré pattern and quantum-wire network of the TBG. When two graphene monolayers (orange) are stacked with a misalignment, there appears a moiré pattern with the wavelength $\lambda = a_0/[2 \sin(\theta/2)]$, monolayer lattice constant a_0 , and the angle θ between the layers. The moiré pattern results in three sets of parallel quantum wires, plotted in distinct colors and labeled by j , with the interwire distance $d = \sqrt{3}\lambda/2$.

AB- and BA-stacking regions [73–75] and form a triangular quantum-wire network illustrated in Fig. 1; we also note spectroscopic [9–11, 76, 77] and transport [78] features of the domain-wall network [79]. These findings motivated theoretical studies on network models based on Luttinger liquids [80–84], reminiscent of earlier works on (crossed) sliding Luttinger liquids proposed for cuprates [85–88] and the coupled-wire constructions of various quantum Hall states [89–99]. From a different perspective, moiré systems provide mesoscopic realizations of coupled-wire systems originally proposed for entirely distinct systems [85–88].

In this work, we extend the network models [80–84] to explore the possibility for topological phases in moiré systems. We construct operators describing general scattering processes based on conservation laws and investigate the resulting electronic states. In moiré structures, the periodic po-

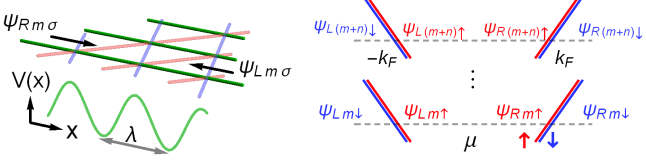


FIG. 2. Quantum-wire network in a moiré structure. Left: For each wire, we define the local coordinate x and fermion fields $\psi_{\ell m \sigma}$, which experience a periodic potential $V(x)$ generated by the moiré structure. Right: Each array consists of parallel wires with the chemical potential μ and Fermi wave vector k_F , where we linearize the energy dispersion and bosonize the fields with Eq. (1).

tential allows for generalized umklapp scatterings, which lead to correlated states at fractional fillings. Remarkably, we identify processes that lead to a gapped bulk with gapless modes along the edges, resembling the observed Chern insulators in TBG [28–35]. Furthermore, we demonstrate that this description can be useful by making concrete predictions for spectroscopic and transport features. In addition to TBG, our mechanism can apply to other nanoscale systems forming arrays of one-dimensional channels, such as twisted moiré bilayers formed by WTe₂ [100] or topological insulators [101, 102], as well as strain-engineered graphene [103].

Bosonization. We introduce the fermion field $\psi_{\ell m \sigma}^{(j)}$ with the array index $j \in \{1, 2, 3\}$, wire index $m \in [1, N_\perp]$ within each array, the index $\ell \in \{R \equiv +, L \equiv -\}$ labeling the moving direction, and spin $\sigma \in \{\uparrow \equiv +, \downarrow \equiv -\}$; see Fig. 2. The fermion field can be bosonized as

$$\psi_{\ell m \sigma}^{(j)}(x) = \frac{U_{\ell m \sigma}^j}{\sqrt{2\pi a}} e^{i\ell k_F x} \times e^{\frac{-i}{\sqrt{2}} [\ell \phi_{cm}^j(x) - \theta_{cm}^j(x) + \ell \sigma \phi_{sm}^j(x) - \sigma \theta_{sm}^j(x)]}, \quad (1)$$

with the Klein factor $U_{\ell m \sigma}^j$, short-distance cutoff a , local coordinate x , Fermi wave vector k_F (identical for all wires), and the index $\xi \in \{c \equiv +, s \equiv -\}$ for the charge/spin sector of the boson fields $\phi_{\xi m}^j$ and $\theta_{\xi m}^j$, satisfying

$$[\phi_{\xi m}^j(x), \theta_{\xi' m'}^{j'}(x')] = i \frac{\pi}{2} \text{sign}(x' - x) \delta_{jj'} \delta_{\xi \xi'} \delta_{mm'}. \quad (2)$$

Below we omit the Klein factor and x whenever possible.

The unperturbed Hamiltonian $H_0 + H_{\text{fs}}$ describes a crossed sliding Luttinger liquid at the fixed point [82], with the kinetic energy H_0 and marginally relevant forward scattering terms H_{fs} quadratic in the density operator $\propto \partial_x \phi_{cm}^j$. In addition, there exist intrawire or interwire backscattering processes, arising from electron-electron interactions and/or tunnelings, which can destabilize the fixed point characterized by the quadratic terms, as those in coupled-wire systems [89–99]. Since the bandwidth W serves as high-energy cutoff [104], the dimensionless coupling g/W , with the strength g characterizing a general scattering, takes a larger value in (quasi-)flat-band systems, allowing for higher-order scatterings to play a more significant role. As in Refs. [89, 95], we do

not specify H_{fs} ; for demonstration, a specific model [82, 85–88] is presented in Supplemental Material (SM) [105]. Below we construct operators describing general scatterings, including higher-order processes (previously discussed in multiband wires [106, 107]), and discuss the resulting electronic states.

General scattering operator. We consider the operator,

$$O_{\{s_{\ell p \sigma}^j\}} = \sum_{m=1}^{N_\perp} \prod_{p=0}^3 \prod_{j=1}^3 [\psi_{R(m+p)\uparrow}^{(j)}]^{s_{R p \uparrow}^j} [\psi_{L(m+p)\uparrow}^{(j)}]^{s_{L p \uparrow}^j} \times [\psi_{R(m+p)\downarrow}^{(j)}]^{s_{R p \downarrow}^j} [\psi_{L(m+p)\downarrow}^{(j)}]^{s_{L p \downarrow}^j}, \quad (3)$$

where the subscript $\{s_{\ell p \sigma}^j\}$ denotes an integer set for all values of (j, ℓ, p, σ) with $p \in \text{integers}$. The set characterizes O ; a negative value implies Hermitian conjugate: $\psi^s \equiv (\psi^\dagger)^{|s|}$ for $s < 0$. A nonzero s for a given p indicates that the p -th nearest neighbor wires participate in the scattering. While O can in principle involve any number of wires, physically one expects s to vanish for large p in systems subject to finite-range interactions.

The operator O describes scatterings within an array when s is nonzero for a single j value. The corresponding renormalization-group (RG) relevance condition is given by $\Delta_{s_{\ell p \sigma}^j} < 2$, where the scaling dimension $\Delta_{s_{\ell p \sigma}^j}$ is determined by $H_0 + H_{\text{fs}}$. In a network consisting of crossed wires, interarray scatterings can occur at wire intersections [81, 82, 87, 88], as characterized by Eq. (3) with nonzero s for multiple j values. Refs. [81, 82] showed that such scatterings can induce superconducting and insulating phases in moiré bilayers. However, the RG relevance condition in this case is more stringent: $\Delta_{s_{\ell p \sigma}^j} < 1$, since the corresponding operator enters the effective action without involving the spatial integral [105]. Furthermore, the interarray scatterings are independent of the filling factor. To explore correlated states from more RG relevant scatterings, below we examine scatterings within an array and suppress j .

We start with the constraints on possible $s_{\ell p \sigma}$ values. In the absence of proximity-induced “external” pairing, the global particle number or charge is conserved, giving

$$\sum_{p, \sigma} (s_{R p \sigma} + s_{L p \sigma}) = 0. \quad (4)$$

For clean systems, the momentum conservation gives additional constraint. Here, the moiré structure plays an important role, as it creates a periodic potential, which partially relaxes the constraint from the momentum conservation. As illustrated in Fig. 2, electrons experience a moiré potential with a spatial period of λ . This leads to a generalized condition for momentum conservation,

$$k_F \sum_{p, \sigma} (s_{R p \sigma} - s_{L p \sigma}) = \frac{2\pi}{\lambda} \times \text{integer}, \quad (5)$$

which allows us to organize $O_{\{s_{\ell p \sigma}\}}$ into two categories.

In the first category, scatterings are allowed for any k_F independent of the filling factor, provided that the coefficients satisfy

$$\sum_{p,\sigma} (s_{Rp\sigma} - s_{Lp\sigma}) = 0. \quad (6)$$

Together with the constraint in Eq. (4), we get

$$\sum_{p,\sigma} s_{Rp\sigma} = \sum_{p,\sigma} s_{Lp\sigma} = 0, \quad (7)$$

meaning that the numbers of the left- and right-moving particles are individually conserved. We refer to these processes as *conventional scatterings*, which characterize electronic states corresponding the “crystalline states” in Ref. [89].

At certain fillings, on the other hand, another category of scatterings can take place even when Eq. (6) is not fulfilled. The momentum difference due to the number imbalance between the left- and right-moving particles can be compensated by the “crystal momentum” proportional to the reciprocal lattice vector $2\pi/\lambda$. With Eqs. (4)–(5) and the relation between the filling factor and Fermi wave vector $\nu = k_F\lambda/\pi$ [104], we get a condition on the filling factor,

$$\nu = \frac{P}{\sum_{p,\sigma} s_{Rp\sigma}}, \quad (8)$$

with a nonzero integer P . In our description, $\nu = 1$ corresponds to 4 electrons per moiré unit cell in TBG [81, 82]. Since these processes are feasible owing to the presence of the moiré periodic potential, in analogy to Refs. [104, 108], we refer to the second category as *moiré umklapp scatterings* and the corresponding states of matter *moiré correlated states*.

For both categories, the bosonization in Eq. (1) gives

$$O_{\{s_{Rp\sigma}\}} = \sum_{m=1} \text{Exp} \left\{ \frac{i}{\sqrt{2}} \sum_p [S_{p,c} \phi_{c(m+p)} + \bar{S}_{p,c} \theta_{c(m+p)} + S_{p,s} \phi_{s(m+p)} + \bar{S}_{p,s} \theta_{s(m+p)}] \right\}, \quad (9)$$

with the coefficients,

$$S_{p,\xi} = s_{Lp\uparrow} - s_{Rp\uparrow} + \xi(s_{Lp\downarrow} - s_{Rp\downarrow}), \quad (10a)$$

$$\bar{S}_{p,\xi} = s_{Lp\uparrow} + s_{Rp\uparrow} + \xi(s_{Lp\downarrow} + s_{Rp\downarrow}). \quad (10b)$$

The global charge conservation requires $\sum_p \bar{S}_{p,c} = 0$. The momentum conservation requires $\sum_p S_{p,c} = 0$ for conventional scatterings and $\nu \sum_p S_{p,c} = 2P$ for moiré umklapp scatterings. If the charge (spin) is conserved for a fixed p , the coefficient $\bar{S}_{p,c}$ ($S_{p,s}$) vanishes. While there is in general no constraint on $\bar{S}_{p,s}$, for simplicity we choose $\bar{S}_{p,s} = 0$, as operators with nonzero $\bar{S}_{p,s}$ are typically less RG relevant.

The conventional scatterings fulfilling Eq. (7) include charge-density-wave couplings, Josephson couplings, and hoppings. They lead to charge density wave, superconducting, and Fermi liquid states, respectively [105]. In addition, the twisted structure enables moiré umklapp scatterings, which we discuss below.

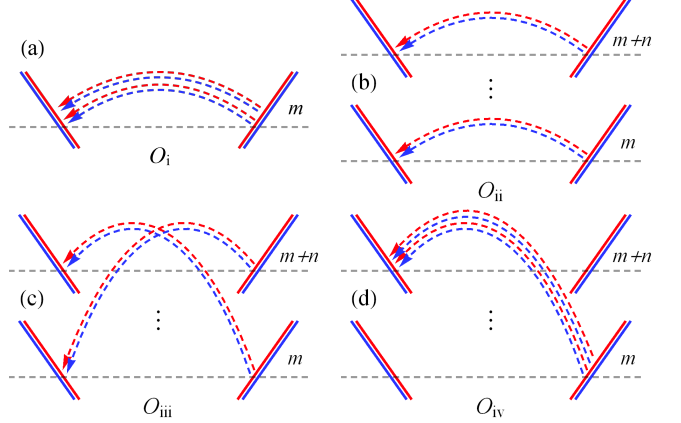


FIG. 3. Examples for moiré umklapp scatterings at $\nu = P/4$. (a) O_i , characterized by Eq. (3) with $(s_{R0\sigma}, s_{L0\sigma}) = (2, -2)$. (b) O_{ii} , with $(s_{R0\sigma}, s_{L0\sigma}, s_{Rn\sigma}, s_{Ln\sigma}) = (1, -1, 1, -1)$. (c) O_{iii} , with $(s_{R0\sigma}, s_{L0\sigma}, s_{Rn\sigma}, s_{Ln\sigma}) = (1, -1, 1, -1)$. (d) O_{iv} , with $(s_{R0\sigma}, s_{L0\sigma}, s_{Rn\sigma}, s_{Ln\sigma}) = (2, 0, 0, -2)$. Here we illustrate processes that are invariant upon changing the spin sign; see Table S1 for more general cases.

Moiré correlated states. The moiré umklapp scatterings can be further categorized into four types, depending on whether they involve multiple wires, whether they involve scatterings between wires, and whether they conserve the particle number for each wire. While the operator in Eq. (3) describes general processes at fractional fillings in Eq. (8), below we provide specific examples allowed at $\nu = P/4$.

We start with processes involving only single wires and denote the corresponding operator as O_i . In Fig. 3(a), we illustrate the process with nonzero coefficients, $(s_{R0\sigma}, s_{L0\sigma}) = (2, -2)$ for both $\sigma = \uparrow$ and $\sigma = \downarrow$. The example describes a process where four electrons at k_F are backscattered to $-k_F$, with the total momentum difference $8k_F = 4\nu \times (2\pi/\lambda)$ compensated by the moiré potential. Next, there are umklapp processes involving multiple wires with correlated intrawire scatterings, labeled as O_{ii} . The simplest case involves two n -th nearest neighboring wires, with an example in Fig. 3(b); we note that the number of backscatterings in each wire can be different. Furthermore, we have O_{iii} involving interwire scatterings while still conserving the particle number for each wire. As mentioned above, the latter constraint implies $\bar{S}_{p,c} = 0$ for any p , as in the case for O_i and O_{ii} . For instance, in Fig. 3(c) we show a process involving two n -th nearest neighbor wires. Finally, allowing for processes which do not conserve the particle number for some wires, we have O_{iv} , with $\bar{S}_{p,c} \neq 0$ for some p . In Fig. 3(d) we plot a two-wire process. In addition to the depicted examples, we present the moiré umklapp scatterings in Table S1 in SM [105], covering a broader range of fillings and higher-order processes.

For O_i , O_{ii} , and O_{iii} , one can obtain a sum of sine-Gordon terms upon bosonization. Taking Fig. 3(a) as an example, we have $O_i + O_i^\dagger \propto \sum_m \cos(4\sqrt{2}\phi_{cm})$. When the corresponding operator is RG relevant, it gaps out all the ϕ_{cm} fields

and leads to a correlated insulating state at fractional fillings. In the strong-coupling limit, ϕ_{cm} is pinned to a minimum of the cosine. A kink excitation corresponds to a tunneling process between two neighboring minima, where ϕ_{cm} changes its value by $\pm\pi/(2\sqrt{2})$. We find that the system hosts fractional excitations with charge $\pm e/2$ associated with the kink. In contrast to the first three types, the states resulting from O_{iv} can host gapless edge modes, which we demonstrate next.

Chiral edge modes. We consider O_{iv} scattering involving the n -th nearest neighbor wires, which allows us to keep only a few nonzero coefficients in Eq. (10); i.e., $S_{n,c} = S_{0,c}$ and $\bar{S}_{n,c} = -\bar{S}_{0,c}$. To proceed, we introduce chiral fields $\Phi_{\ell m} = -\ell\phi_{cm} + f\theta_{cm}$ with $f = -\bar{S}_{0,c}/S_{0,c}$, which satisfy

$$[\Phi_{\ell m}(x), \Phi_{\ell' m'}(x')] = i\ell\pi\delta_{\ell\ell'}\delta_{mm'}f \text{ sign}(x - x'). \quad (11)$$

The transformation leads to

$$O_{iv} + O_{iv}^\dagger \propto \sum_{m=1} \cos \left\{ \frac{S_{0,c}}{\sqrt{2}} [\Phi_{L(m+n)} - \Phi_{Rm}] \right\}. \quad (12)$$

The expression indicates the presence of n gapless chiral modes $\Phi_{L,1}, \dots, \Phi_{L,n}$ at one edge and, similarly, n gapless right-moving modes at the opposite edge. To proceed, we define $\tilde{\Phi}_{m,n} = [\Phi_{L(m+n)} - \Phi_{Rm}]/2$ and get $O_{iv} + O_{iv}^\dagger \propto \sum_{m=1} \cos(\sqrt{2}S_{0,c}\tilde{\Phi}_{m,n})$. Using Eq. (11), it can be shown that the $\tilde{\Phi}_{m,n}$ fields for any m commute [105], gapping out the bulk modes in the interior of the system. Similar to the correlated states induced by O_i – O_{iii} , the system hosts fractional excitations, with charge $\pm 2e/S_{0,c}$. We expect formation of chirality domains, hosting gapless chiral modes at domain walls [105]. While the formation of domain walls costs energy, (disorder-induced) local magnetic moments can trigger their formation, which increases the entropy and therefore lowers the free energy at finite temperatures. Remarkably, a finite magnetic field is required to train domains in order to stabilize edge modes with a definite chirality in micrometer-size samples [28, 29].

Using the Landauer-Büttiker formalism [109–112], we obtain quantized Hall resistance $h/(ne^2)$. For $n = 1$ and $\nu = 3/4$, it leads to a value of h/e^2 , as observed in Ref. [29]. In consequence, the system exhibits quantum anomalous Hall effect with chiral edge modes and fractional excitations. We note that it is possible to reproduce a sequence of Chern insulating states with $C = \pm 1, \pm 2$ and ± 3 (corresponding to n here) at fillings $\nu = \pm 3/4, \pm 1/2$ and $\pm 1/4$, respectively. The complete sequence was observed in Refs. [30–32], while a partial set was reported in Refs. [27–29, 33–36].

To demonstrate that O_{iv} can be RG relevant, we compute its scaling dimension and get [105]

$$\Delta_{iv} = \frac{1}{2} |S_{0,c}\bar{S}_{0,c}| \left(1 + \frac{2U}{\hbar v_0} \right)^{-\frac{1}{2}}, \quad (13)$$

with the $q \sim 0$ Fourier component U of the density-density interaction and the velocity v_0 . In consequence, for a given scattering process, the RG relevance condition $\Delta_{iv} < 2$ is fulfilled for sufficiently large U .

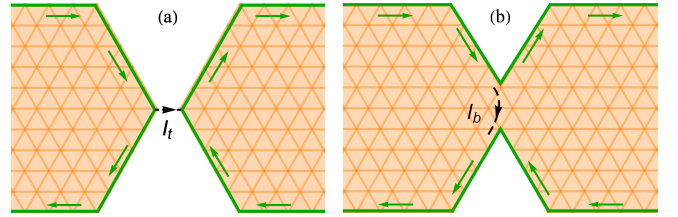


FIG. 4. QPC setups for systems in a moiré correlated state with a gapped bulk (orange) and gapless chiral edge modes (green). The setup (a) allows for tunnel current I_t . The setup (b) leads to backscattering current I_b and conductance correction δG .

Experimental signatures. The predicted chiral edge modes can be characterized by spectroscopic and transport measurements. For simplicity we consider a moiré correlated state hosting a single edge mode [105]. Utilizing scanning tunneling spectroscopy, one can probe the local density of states, which follows a universal scaling curve for energy ϵ and temperature T ,

$$\rho(\epsilon) \propto T^{\frac{1}{f}-1} \cosh\left(\frac{\epsilon}{2k_B T}\right) \left| \Gamma\left(\frac{1}{2f} + i\frac{\epsilon}{2\pi k_B T}\right) \right|^2. \quad (14)$$

In contrast to carbon nanotubes [113, 114] or helical liquids [115, 116], the scaling exponent here does not depend on H_{fs} , demonstrating the topological nature of the chiral edge modes.

Alternatively, one can probe the chiral edge modes via charge transport [117–122]. Specifically, we consider two setups employing quantum point contacts (QPCs). The setup in Fig. 4(a) allows for interedge tunneling with a current described by another universal scaling formula,

$$I_t \propto T^{\frac{2}{f}-1} \sinh\left(\frac{eV}{2k_B T}\right) \left| \Gamma\left(\frac{1}{f} + i\frac{eV}{2\pi k_B T}\right) \right|^2, \quad (15)$$

with bias voltage V . On the other hand, the interedge backscattering in Fig. 4(b) leads to power-law correction in the (differential) conductance with the magnitude $|\delta G| \propto \max(eV, k_B T)^{2f-2}$. Unlike fractional quantum Hall states [117–121], the scaling exponents depend on f here, but not directly on the filling factor ν . The same QPC geometry can be used to detect fractional charges through shot noise [123–125].

As a remark, while the theoretical works establishing the quantum-wire network in moiré bilayers [73, 75] involve a sufficiently large interlayer potential difference, achievable via voltage gates, we expect that the network can form under broader conditions [9–11, 76–78]. Namely, a spectral gap can be generally induced in graphene-based devices through coupling to other layered materials or substrates, depending on their stacking configurations [27–29, 36, 126–130]. Therefore, a gap with a spatially dependent sign can be achieved through nanoscale engineering [82, 103, 131], leading to a network of gapless domain walls that separate regions with opposing gap signs.

Finally, we point out that, through the proposed experimental verification, the system can reveal the long-sought intrinsic fractional quantum anomalous Hall states, where topology and many-body physics interplay. Upon inducing superconductivity (e.g., by proximity), moiré correlated states hosting fractional edge modes provide a platform to stabilize parafermion edge or zero modes [132–141] even without magnetic fields.

Acknowledgments. We thank Y.-Y. Chang, C.-H. Chung, and C.-T. Ke for interesting discussions. This work was financially supported by the JSPS Kakenhi Grant No. 19H05610, the Swiss National Science Foundation (Switzerland), the NCCR QSIT, and the National Science and Technology Council (NSTC), Taiwan through NSTC-112-2112-M-001-025-MY3.

-
- [1] E. Y. Andrei and A. H. MacDonald, Graphene bilayers with a twist, *Nat. Mater.* **19**, 1265 (2020).
- [2] L. Balents, C. R. Dean, D. K. Efetov, and A. F. Young, Superconductivity and strong correlations in moiré flat bands, *Nat. Phys.* **16**, 725 (2020).
- [3] E. Y. Andrei, D. K. Efetov, P. Jarillo-Herrero, A. H. MacDonald, K. F. Mak, T. Senthil, E. Tutuc, A. Yazdani, and A. F. Young, The marvels of moiré materials, *Nat. Rev. Mater.* **6**, 201 (2021).
- [4] D. M. Kennes, M. Claassen, L. Xian, A. Georges, A. J. Millis, J. Hone, C. R. Dean, D. N. Basov, A. N. Pasupathy, and A. Rubio, Moiré heterostructures as a condensed-matter quantum simulator, *Nat. Phys.* **17**, 155 (2021).
- [5] R. Bistritzer and A. H. MacDonald, Moiré bands in twisted double-layer graphene, *Proc. Natl. Acad. Sci. USA* **108**, 12233 (2011).
- [6] Y. Cao, V. Fatemi, S. Fang, K. Watanabe, T. Taniguchi, E. Kaxiras, and P. Jarillo-Herrero, Unconventional superconductivity in magic-angle graphene superlattices, *Nature* **556**, 43 (2018).
- [7] Y. Cao, V. Fatemi, A. Demir, S. Fang, S. L. Tomarken, J. Y. Luo, J. D. Sanchez-Yamagishi, K. Watanabe, T. Taniguchi, E. Kaxiras, R. C. Ashoori, and P. Jarillo-Herrero, Correlated insulator behaviour at half-filling in magic-angle graphene superlattices, *Nature* **556**, 80 (2018).
- [8] We additionally note an earlier experimental study on the electronic structure of moiré MoS₂/WSe₂ heterobilayers [142].
- [9] Y. Choi, J. Kemmer, Y. Peng, A. Thomson, H. Arora, R. Polski, Y. Zhang, H. Ren, J. Alicea, G. Refael, F. von Oppen, K. Watanabe, T. Taniguchi, and S. Nadj-Perge, Electronic correlations in twisted bilayer graphene near the magic angle, *Nat. Phys.* **15**, 1174 (2019).
- [10] Y. Jiang, X. Lai, K. Watanabe, T. Taniguchi, K. Haule, J. Mao, and E. Y. Andrei, Charge order and broken rotational symmetry in magic-angle twisted bilayer graphene, *Nature* **573**, 91 (2019).
- [11] A. Kerelsky, L. J. McGilly, D. M. Kennes, L. Xian, M. Yankowitz, S. Chen, K. Watanabe, T. Taniguchi, J. Hone, C. Dean, A. Rubio, and A. N. Pasupathy, Maximized electron interactions at the magic angle in twisted bilayer graphene, *Nature* **572**, 95 (2019).
- [12] Y. Cao, D. Rodan-Legrain, J. M. Park, F. N. Yuan, K. Watanabe, T. Taniguchi, R. M. Fernandes, L. Fu, and P. Jarillo-Herrero, Nematicity and Competing Orders in Superconducting Magic-Angle Graphene, *Science* **372**, 264 (2021).
- [13] M. Yankowitz, S. Chen, H. Polshyn, Y. Zhang, K. Watanabe, T. Taniguchi, D. Graf, A. F. Young, and C. R. Dean, Tuning superconductivity in twisted bilayer graphene, *Science* **363**, 1059 (2019).
- [14] H. Polshyn, M. Yankowitz, S. Chen, Y. Zhang, K. Watanabe, T. Taniguchi, C. R. Dean, and A. F. Young, Large linear-in-temperature resistivity in twisted bilayer graphene, *Nat. Phys.* **15**, 1011 (2019).
- [15] Y. Cao, D. Chowdhury, D. Rodan-Legrain, O. Rubies-Bigorda, K. Watanabe, T. Taniguchi, T. Senthil, and P. Jarillo-Herrero, Strange Metal in Magic-Angle Graphene with near Planckian Dissipation, *Phys. Rev. Lett.* **124**, 076801 (2020).
- [16] D. Wong, K. P. Nuckolls, M. Oh, B. Lian, Y. Xie, S. Jeon, K. Watanabe, T. Taniguchi, B. A. Bernevig, and A. Yazdani, Cascade of electronic transitions in magic-angle twisted bilayer graphene, *Nature* **582**, 198 (2020).
- [17] U. Zondiner, A. Rozen, D. Rodan-Legrain, Y. Cao, R. Queiroz, T. Taniguchi, K. Watanabe, Y. Oreg, F. von Oppen, A. Stern, E. Berg, P. Jarillo-Herrero, and S. Ilani, Cascade of phase transitions and Dirac revivals in magic-angle graphene, *Nature* **582**, 203 (2020).
- [18] X. Lu, P. Stepanov, W. Yang, M. Xie, M. A. Aamir, I. Das, C. Urgell, K. Watanabe, T. Taniguchi, G. Zhang, A. Bachtold, A. H. MacDonald, and D. K. Efetov, Superconductors, orbital magnets and correlated states in magic-angle bilayer graphene, *Nature* **574**, 653 (2019).
- [19] A. L. Sharpe, E. J. Fox, A. W. Barnard, J. Finney, K. Watanabe, T. Taniguchi, M. A. Kastner, and D. Goldhaber-Gordon, Evidence of Orbital Ferromagnetism in Twisted Bilayer Graphene Aligned to Hexagonal Boron Nitride, *Nano Lett.* **21**, 4299 (2021).
- [20] H. S. Arora, R. Polski, Y. Zhang, A. Thomson, Y. Choi, H. Kim, Z. Lin, I. Z. Wilson, X. Xu, J.-H. Chu, K. Watanabe, T. Taniguchi, J. Alicea, and S. Nadj-Perge, Superconductivity in metallic twisted bilayer graphene stabilized by WSe₂, *Nature* **583**, 379 (2020).
- [21] Y. Saito, J. Ge, K. Watanabe, T. Taniguchi, and A. F. Young, Independent superconductors and correlated insulators in twisted bilayer graphene, *Nat. Phys.* **16**, 926 (2020).
- [22] P. Stepanov, I. Das, X. Lu, A. Fahimniya, K. Watanabe, T. Taniguchi, F. H. L. Koppens, J. Lischner, L. Levitov, and D. K. Efetov, Untying the insulating and superconducting orders in magic-angle graphene, *Nature* **583**, 375 (2020).
- [23] A. Uri, S. Grover, Y. Cao, J. A. Crosse, K. Bagani, D. Rodan-Legrain, Y. Myasoedov, K. Watanabe, T. Taniguchi, P. Moon, M. Koshino, P. Jarillo-Herrero, and E. Zeldov, Mapping the twist-angle disorder and Landau levels in magic-angle graphene, *Nature* **581**, 47 (2020).
- [24] Y. Saito, F. Yang, J. Ge, X. Liu, T. Taniguchi, K. Watanabe, J. I. A. Li, E. Berg, and A. F. Young, Isospin Pomeranchuk effect in twisted bilayer graphene, *Nature* **592**, 220 (2021).
- [25] A. Rozen, J. M. Park, U. Zondiner, Y. Cao, D. Rodan-Legrain, T. Taniguchi, K. Watanabe, Y. Oreg, A. Stern, E. Berg, P. Jarillo-Herrero, and S. Ilani, Entropic evidence for a Pomeranchuk effect in magic-angle graphene, *Nature* **592**, 214 (2021).
- [26] M. Oh, K. P. Nuckolls, D. Wong, R. L. Lee, X. Liu, K. Watanabe, T. Taniguchi, and A. Yazdani, Evidence for unconventional superconductivity in twisted bilayer graphene, *Nature* **600**, 240 (2021).
- [27] J.-X. Lin, Y.-H. Zhang, E. Morissette, Z. Wang, S. Liu, D. Rhodes, K. Watanabe, T. Taniguchi, J. Hone, and J. I. A. Li, Spin-orbit-driven ferromagnetism at half moiré filling in magic-angle twisted bilayer graphene, *Science* **375**, 437 (2022).

- [28] A. L. Sharpe, E. J. Fox, A. W. Barnard, J. Finney, K. Watanabe, T. Taniguchi, M. A. Kastner, and D. Goldhaber-Gordon, Emergent ferromagnetism near three-quarters filling in twisted bilayer graphene, *Science* **365**, 605 (2019).
- [29] M. Serlin, C. L. Tschirhart, H. Polshyn, Y. Zhang, J. Zhu, K. Watanabe, T. Taniguchi, L. Balents, and A. F. Young, Intrinsic quantized anomalous Hall effect in a moiré heterostructure, *Science* **367**, 900 (2020).
- [30] K. P. Nuckolls, M. Oh, D. Wong, B. Lian, K. Watanabe, T. Taniguchi, B. A. Bernevig, and A. Yazdani, Strongly correlated Chern insulators in magic-angle twisted bilayer graphene, *Nature* **588**, 610 (2020).
- [31] Y. Choi, H. Kim, Y. Peng, A. Thomson, C. Lewandowski, R. Polski, Y. Zhang, H. S. Arora, K. Watanabe, T. Taniguchi, J. Alicea, and S. Nadj-Perge, Correlation-driven topological phases in magic-angle twisted bilayer graphene, *Nature* **589**, 536 (2021).
- [32] I. Das, X. Lu, J. Herzog-Arbeitman, Z.-D. Song, K. Watanabe, T. Taniguchi, B. A. Bernevig, and D. K. Efetov, Symmetry-broken Chern insulators and Rashba-like Landau-level crossings in magic-angle bilayer graphene, *Nat. Phys.* **17**, 710 (2021).
- [33] Y. Saito, J. Ge, L. Rademaker, K. Watanabe, T. Taniguchi, D. A. Abanin, and A. F. Young, Hofstadter subband ferromagnetism and symmetry-broken Chern insulators in twisted bilayer graphene, *Nat. Phys.* **17**, 478 (2021).
- [34] P. Stepanov, M. Xie, T. Taniguchi, K. Watanabe, X. Lu, A. H. MacDonald, B. A. Bernevig, and D. K. Efetov, Competing Zero-Field Chern Insulators in Superconducting Twisted Bilayer Graphene, *Phys. Rev. Lett.* **127**, 197701 (2021).
- [35] J. M. Park, Y. Cao, K. Watanabe, T. Taniguchi, and P. Jarillo-Herrero, Flavour Hund's coupling, Chern gaps and charge diffusivity in moiré graphene, *Nature* **592**, 43 (2021).
- [36] C.-C. Tseng, X. Ma, Z. Liu, K. Watanabe, T. Taniguchi, J.-H. Chu, and M. Yankowitz, Anomalous Hall Effect at Half Filling in Twisted Bilayer Graphene, *Nat. Phys.* **18**, 1038 (2022).
- [37] D. M. Kennes, J. Lischner, and C. Karrasch, Strong correlations and $d+id$ superconductivity in twisted bilayer graphene, *Phys. Rev. B* **98**, 241407(R) (2018).
- [38] M. Koshino, N. F. Q. Yuan, T. Koretsune, M. Ochi, K. Kuroki, and L. Fu, Maximally Localized Wannier Orbitals and the Extended Hubbard Model for Twisted Bilayer Graphene, *Phys. Rev. X* **8**, 031087 (2018).
- [39] H. C. Po, L. Zou, A. Vishwanath, and T. Senthil, Origin of Mott Insulating Behavior and Superconductivity in Twisted Bilayer Graphene, *Phys. Rev. X* **8**, 031089 (2018).
- [40] F. Wu, A. H. MacDonald, and I. Martin, Theory of Phonon-Mediated Superconductivity in Twisted Bilayer Graphene, *Phys. Rev. Lett.* **121**, 257001 (2018).
- [41] J. Kang and O. Vafek, Strong Coupling Phases of Partially Filled Twisted Bilayer Graphene Narrow Bands, *Phys. Rev. Lett.* **122**, 246401 (2019).
- [42] B. Lian, Z. Wang, and B. A. Bernevig, Twisted Bilayer Graphene: A Phonon-Driven Superconductor, *Phys. Rev. Lett.* **122**, 257002 (2019).
- [43] K. Seo, V. N. Kotov, and B. Uchoa, Ferromagnetic Mott state in Twisted Graphene Bilayers at the Magic Angle, *Phys. Rev. Lett.* **122**, 246402 (2019).
- [44] N. Bultinck, S. Chatterjee, and M. P. Zaletel, Mechanism for Anomalous Hall Ferromagnetism in Twisted Bilayer Graphene, *Phys. Rev. Lett.* **124**, 166601 (2020).
- [45] N. Bultinck, E. Khalaf, S. Liu, S. Chatterjee, A. Vishwanath, and M. P. Zaletel, Ground State and Hidden Symmetry of Magic-Angle Graphene at Even Integer Filling, *Phys. Rev. X* **10**, 031034 (2020).
- [46] M. Christos, S. Sachdev, and M. S. Scheurer, Superconductivity, correlated insulators, and Wess-Zumino-Witten terms in twisted bilayer graphene, *Proc. Natl. Acad. Sci. USA* **117**, 29543 (2020).
- [47] M. Xie and A. H. MacDonald, Nature of the Correlated Insulator States in Twisted Bilayer Graphene, *Phys. Rev. Lett.* **124**, 097601 (2020).
- [48] K. Hejazi, X. Chen, and L. Balents, Hybrid Wannier Chern bands in magic angle twisted bilayer graphene and the quantized anomalous Hall effect, *Phys. Rev. Research* **3**, 013242 (2021).
- [49] E. Khalaf, S. Chatterjee, N. Bultinck, M. P. Zaletel, and A. Vishwanath, Charged skyrmions and topological origin of superconductivity in magic-angle graphene, *Sci. Adv.* **7**, eabf5299 (2021).
- [50] S. Liu, E. Khalaf, J. Y. Lee, and A. Vishwanath, Nematic topological semimetal and insulator in magic-angle bilayer graphene at charge neutrality, *Phys. Rev. Research* **3**, 013033 (2021).
- [51] D. E. Parker, T. Soejima, J. Hauschild, M. P. Zaletel, and N. Bultinck, Strain-Induced Quantum Phase Transitions in Magic-Angle Graphene, *Phys. Rev. Lett.* **127**, 027601 (2021).
- [52] G. Shavit, E. Berg, A. Stern, and Y. Oreg, Theory of Correlated Insulators and Superconductivity in Twisted Bilayer Graphene, *Phys. Rev. Lett.* **127**, 247703 (2021).
- [53] G. Wagner, Y. H. Kwan, N. Bultinck, S. H. Simon, and S. A. Parameswaran, Global Phase Diagram of the Normal State of Twisted Bilayer Graphene, *Phys. Rev. Lett.* **128**, 156401 (2022).
- [54] G. W. Burg, J. Zhu, T. Taniguchi, K. Watanabe, A. H. MacDonald, and E. Tutuc, Correlated Insulating States in Twisted Double Bilayer Graphene, *Phys. Rev. Lett.* **123**, 197702 (2019).
- [55] G. Chen, A. L. Sharpe, P. Gallagher, I. T. Rosen, E. J. Fox, L. Jiang, B. Lyu, H. Li, K. Watanabe, T. Taniguchi, J. Jung, Z. Shi, D. Goldhaber-Gordon, Y. Zhang, and F. Wang, Signatures of tunable superconductivity in a trilayer graphene moiré superlattice, *Nature* **572**, 215 (2019).
- [56] G. Chen, L. Jiang, S. Wu, B. Lyu, H. Li, B. L. Chittari, K. Watanabe, T. Taniguchi, Z. Shi, J. Jung, Y. Zhang, and F. Wang, Evidence of a gate-tunable Mott insulator in a trilayer graphene moiré superlattice, *Nat. Phys.* **15**, 237 (2019).
- [57] Y. Cao, D. Rodan-Legrain, O. Rubies-Bigorda, J. M. Park, K. Watanabe, T. Taniguchi, and P. Jarillo-Herrero, Tunable correlated states and spin-polarized phases in twisted bilayer-bilayer graphene, *Nature* **583**, 215 (2020).
- [58] Y. Cao, J. M. Park, K. Watanabe, T. Taniguchi, and P. Jarillo-Herrero, Large Pauli Limit Violation and Reentrant Superconductivity in Magic-Angle Twisted Trilayer Graphene, (2021), arXiv:2103.12083.
- [59] X. Liu, Z. Hao, E. Khalaf, J. Y. Lee, Y. Ronen, H. Yoo, D. H. Najafabadi, K. Watanabe, T. Taniguchi, A. Vishwanath, and P. Kim, Tunable spin-polarized correlated states in twisted double bilayer graphene, *Nature* **583**, 221 (2020).
- [60] C. Shen, Y. Chu, Q. Wu, N. Li, S. Wang, Y. Zhao, J. Tang, J. Liu, J. Tian, K. Watanabe, T. Taniguchi, R. Yang, Z. Y. Meng, D. Shi, O. V. Yazyev, and G. Zhang, Correlated states in twisted double bilayer graphene, *Nat. Phys.* **16**, 520 (2020).
- [61] Z. Hao, A. M. Zimmerman, P. Ledwith, E. Khalaf, D. H. Najafabadi, K. Watanabe, T. Taniguchi, A. Vishwanath, and P. Kim, Electric field-tunable superconductivity in alternating-twist magic-angle trilayer graphene, *Science* **371**, 1133 (2021).
- [62] X. Liu, Z. Wang, K. Watanabe, T. Taniguchi, O. Vafek, and J. I. A. Li, Tuning electron correlation in magic-angle twisted

- bilayer graphene using Coulomb screening, *Science* **371**, 1261 (2021).
- [63] J. M. Park, Y. Cao, K. Watanabe, T. Taniguchi, and P. Jarillo-Herrero, Tunable strongly coupled superconductivity in magic-angle twisted trilayer graphene, *Nature* **590**, 249 (2021).
- [64] E. C. Regan, D. Wang, C. Jin, M. I. B. Utama, B. Gao, X. Wei, S. Zhao, W. Zhao, Z. Zhang, K. Yumigeta, M. Blei, J. D. Carlström, K. Watanabe, T. Taniguchi, S. Tongay, M. Crommie, A. Zettl, and F. Wang, Mott and generalized Wigner crystal states in WSe₂/WS₂ moiré superlattices, *Nature* **579**, 359 (2020).
- [65] Y. Shimazaki, I. Schwartz, K. Watanabe, T. Taniguchi, M. Kroener, and A. Imamoğlu, Strongly correlated electrons and hybrid excitons in a moiré heterostructure, *Nature* **580**, 472 (2020).
- [66] Y. Tang, L. Li, T. Li, Y. Xu, S. Liu, K. Barmak, K. Watanabe, T. Taniguchi, A. H. MacDonald, J. Shan, and K. F. Mak, Simulation of Hubbard model physics in WSe₂/WS₂ moiré superlattices. *Nature* **579**, 353 (2020).
- [67] L. Wang, E.-M. Shih, A. Ghiotto, L. Xian, D. A. Rhodes, C. Tan, M. Claassen, D. M. Kennes, Y. Bai, B. Kim, K. Watanabe, T. Taniguchi, X. Zhu, J. Hone, A. Rubio, A. N. Pasupathy, and C. R. Dean, Correlated electronic phases in twisted bilayer transition metal dichalcogenides, *Nat. Mater.* **19**, 861 (2020).
- [68] Y. Xu, S. Liu, D. A. Rhodes, K. Watanabe, T. Taniguchi, J. Hone, V. Elser, K. F. Mak, and J. Shan, Correlated insulating states at fractional fillings of moiré superlattices, *Nature* **587**, 214 (2020).
- [69] Z. Zhang, Y. Wang, K. Watanabe, T. Taniguchi, K. Ueno, E. Tutuc, and B. J. LeRoy, Flat bands in twisted bilayer transition metal dichalcogenides, *Nat. Phys.* **16**, 1093 (2020).
- [70] S. Tomonaga, Remarks on Bloch's Method of Sound Waves applied to Many-Fermion Problems, *Prog. Theor. Phys.* **5**, 544 (1950).
- [71] J. M. Luttinger, An Exactly Soluble Model of a Many-Fermion System, *J. Math. Phys.* **4**, 1154 (1963).
- [72] F. D. M. Haldane, Luttinger liquid theory of one-dimensional quantum fluids. I. Properties of the Luttinger model and their extension to the general 1D interacting spinless Fermi gas, *J. Phys. C: Solid State Physics* **14**, 2585 (1981).
- [73] P. San-Jose and E. Prada, Helical networks in twisted bilayer graphene under interlayer bias, *Phys. Rev. B* **88**, 121408 (2013).
- [74] N. N. T. Nam and M. Koshino, Lattice relaxation and energy band modulation in twisted bilayer graphene, *Phys. Rev. B* **96**, 075311 (2017).
- [75] D. K. Efimkin and A. H. MacDonald, Helical network model for twisted bilayer graphene, *Phys. Rev. B* **98**, 035404 (2018).
- [76] S. Huang, K. Kim, D. K. Efimkin, T. Lovorn, T. Taniguchi, K. Watanabe, A. H. MacDonald, E. Tutuc, and B. J. LeRoy, Topologically Protected Helical States in Minimally Twisted Bilayer Graphene, *Phys. Rev. Lett.* **121**, 037702 (2018).
- [77] Y. Xie, B. Lian, B. Jäck, X. Liu, C.-L. Chiu, K. Watanabe, T. Taniguchi, B. A. Bernevig, and A. Yazdani, Spectroscopic signatures of many-body correlations in magic-angle twisted bilayer graphene, *Nature* **572**, 101 (2019).
- [78] P. Rickhaus, J. Wallbank, S. Slizovskiy, R. Pisoni, H. Overweg, Y. Lee, M. Eich, M.-H. Liu, K. Watanabe, T. Taniguchi, T. Ihn, and K. Ensslin, Transport Through a Network of Topological Channels in Twisted Bilayer Graphene, *Nano Lett.* **18**, 6725 (2018).
- [79] The STM experiments revealed additional features around AA-stacking regions, which inspired Refs. [143–145] to construct a heavy-fermion model.
- [80] X.-C. Wu, C.-M. Jian, and C. Xu, Coupled-wire description of the correlated physics in twisted bilayer graphene, *Phys. Rev. B* **99**, 161405(R) (2019).
- [81] Y.-Z. Chou, Y.-P. Lin, S. Das Sarma, and R. M. Nandkishore, Superconductor versus insulator in twisted bilayer graphene, *Phys. Rev. B* **100**, 115128 (2019).
- [82] C. Chen, A. H. Castro Neto, and V. M. Pereira, Correlated states of a triangular net of coupled quantum wires: Implications for the phase diagram of marginally twisted bilayer graphene, *Phys. Rev. B* **101**, 165431 (2020).
- [83] Y.-Z. Chou, F. Wu, and J. D. Sau, Charge density wave and finite-temperature transport in minimally twisted bilayer graphene, *Phys. Rev. B* **104**, 045146 (2021).
- [84] J. M. Lee, M. Oshikawa, and G. Y. Cho, Non-Fermi Liquids in Conducting Two-Dimensional Networks, *Phys. Rev. Lett.* **126**, 186601 (2021).
- [85] V. J. Emery, E. Fradkin, S. A. Kivelson, and T. C. Lubensky, Quantum Theory of the Smectic Metal State in Stripe Phases, *Phys. Rev. Lett.* **85**, 2160 (2000).
- [86] A. Vishwanath and D. Carpentier, Two-Dimensional Anisotropic Non-Fermi-Liquid Phase of Coupled Luttinger Liquids, *Phys. Rev. Lett.* **86**, 676 (2001).
- [87] R. Mukhopadhyay, C. L. Kane, and T. C. Lubensky, Crossed sliding Luttinger liquid phase, *Phys. Rev. B* **63**, 081103(R) (2001).
- [88] R. Mukhopadhyay, C. L. Kane, and T. C. Lubensky, Sliding Luttinger liquid phases, *Phys. Rev. B* **64**, 045120 (2001).
- [89] C. L. Kane, R. Mukhopadhyay, and T. C. Lubensky, Fractional Quantum Hall Effect in an Array of Quantum Wires, *Phys. Rev. Lett.* **88**, 036401 (2002).
- [90] J. Klinovaja and D. Loss, Topological Edge States and Fractional Quantum Hall Effect from Umklapp Scattering, *Phys. Rev. Lett.* **111**, 196401 (2013).
- [91] J. Klinovaja and Y. Tserkovnyak, Quantum spin Hall effect in strip of stripes model, *Phys. Rev. B* **90**, 115426 (2014).
- [92] J. Klinovaja and D. Loss, Integer and fractional quantum Hall effect in a strip of stripes, *Eur. Phys. J. B* **87**, 171 (2014).
- [93] T. Neupert, C. Chamon, C. Mudry, and R. Thomale, Wire deconstructionism of two-dimensional topological phases, *Phys. Rev. B* **90**, 205101 (2014).
- [94] E. Sagi and Y. Oreg, Non-Abelian topological insulators from an array of quantum wires, *Phys. Rev. B* **90**, 201102(R) (2014).
- [95] J. C. Y. Teo and C. L. Kane, From Luttinger liquid to non-Abelian quantum Hall states, *Phys. Rev. B* **89**, 085101 (2014).
- [96] J. Klinovaja, Y. Tserkovnyak, and D. Loss, Integer and fractional quantum anomalous Hall effect in a strip of stripes model, *Phys. Rev. B* **91**, 085426 (2015).
- [97] R. A. Santos, C.-W. Huang, Y. Gefen, and D. B. Gutman, Fractional topological insulators: From sliding Luttinger liquids to Chern-Simons theory, *Phys. Rev. B* **91**, 205141 (2015).
- [98] Y. Imamura, K. Totsuka, and T. H. Hansson, From coupled-wire construction of quantum Hall states to wave functions and hydrodynamics, *Phys. Rev. B* **100**, 125148 (2019).
- [99] T. Meng, Coupled-wire constructions: a Luttinger liquid approach to topology, *Eur. Phys. J. Spec. Top.* **229**, 527 (2020).
- [100] P. Wang, G. Yu, Y. H. Kwan, Y. Jia, S. Lei, S. Kleimenz, F. A. Cevallos, R. Singha, T. Devakul, K. Watanabe, T. Taniguchi, S. L. Sondhi, R. J. Cava, L. M. Schoop, S. A. Parameswaran, and S. Wu, One-dimensional Luttinger liquids in a two-dimensional moiré lattice, *Nature* **605**, 57 (2022).
- [101] M. Fujimoto, T. Kawakami, and M. Koshino, Perfect one-dimensional interface states in a twisted stack of three-dimensional topological insulators, *Phys. Rev. Research* **4**, 043209 (2022).
- [102] I. Tateishi and M. Hirayama, Quantum spin Hall effect from multiscale band inversion in twisted bilayer Bi₂(Te_{1-x}Se_x)₃,

- Phys. Rev. Research **4**, 043045 (2022).
- [103] C.-C. Hsu, M. L. Teague, J.-Q. Wang, and N.-C. Yeh, Nanoscale strain engineering of giant pseudo-magnetic fields, valley polarization, and topological channels in graphene, *Sci. Adv.* **6**, eaat9488 (2020).
- [104] T. Giamarchi, *Quantum Physics in One Dimension* (Oxford University Press, New York, 2003).
- [105] See Supplemental Material at [URL will be inserted by publisher] for technical details, which includes Refs. [146, 147].
- [106] G. Shavit and Y. Oreg, Fractional Conductance in Strongly Interacting 1D Systems, *Phys. Rev. Lett.* **123**, 036803 (2019).
- [107] C.-H. Hsu, F. Ronetti, P. Stano, J. Klinovaja, and D. Loss, Universal conductance dips and fractional excitations in a two-subband quantum wire, *Phys. Rev. Research* **2**, 043208 (2020).
- [108] T. Giamarchi, Umklapp process and resistivity in one-dimensional fermion systems, *Phys. Rev. B* **44**, 2905 (1991).
- [109] R. Landauer, Spatial Variation of Currents and Fields Due to Localized Scatterers in Metallic Conduction, *IBM J. Res. Dev.* **1**, 223 (1957).
- [110] R. Landauer, Electrical resistance of disordered one-dimensional lattices, *Philos. Mag.* **21**, 863 (1970).
- [111] M. Büttiker, Absence of backscattering in the quantum Hall effect in multiprobe conductors, *Phys. Rev. B* **38**, 9375 (1988).
- [112] S. Datta, *Electronic Transport in Mesoscopic Systems* (Cambridge University Press, 1995).
- [113] M. Bockrath, D. H. Cobden, J. Lu, A. G. Rinzler, R. E. Smalley, L. Balents, and P. L. McEuen, Luttinger-liquid behaviour in carbon nanotubes, *Nature (London)* **397**, 598 (1999).
- [114] L. Balents, Orthogonality Catastrophes in Carbon Nanotubes, (1999), 10.48550/arXiv.cond-mat/9906032, cond-mat/9906032.
- [115] R. Stühler, F. Reis, T. Müller, T. Helbig, T. Schwemmer, R. Thomale, J. Schäfer, and R. Claessen, Tomonaga-Luttinger liquid in the edge channels of a quantum spin Hall insulator, *Nat. Phys.* **16**, 47 (2019).
- [116] C.-H. Hsu, P. Stano, J. Klinovaja, and D. Loss, Helical liquids in semiconductors, *Semicond. Sci. Technol.* **36**, 123003 (2021).
- [117] C. L. Kane, M. P. A. Fisher, and J. Polchinski, Randomness at the edge: Theory of quantum Hall transport at filling $\nu = 2/3$, *Phys. Rev. Lett.* **72**, 4129 (1994).
- [118] C. L. Kane and M. P. A. Fisher, Impurity scattering and transport of fractional quantum Hall edge states, *Phys. Rev. B* **51**, 13449 (1995).
- [119] C. L. Kane and M. P. A. Fisher, Edge-State Transport, in *Perspectives in Quantum Hall Effects*, edited by S. D. Sarma and A. Pinczuk (John Wiley & Sons, Ltd, 1996) Chap. 4, pp. 109–159.
- [120] M. P. A. Fisher and L. I. Glazman, Transport in a One-Dimensional Luttinger Liquid, in *Mesoscopic Electron Transport*, edited by L. L. Sohn, L. P. Kouwenhoven, and G. Schön (Springer Netherlands, 1997) pp. 331–373.
- [121] A. M. Chang, Chiral Luttinger liquids at the fractional quantum Hall edge, *Rev. Mod. Phys.* **75**, 1449 (2003).
- [122] C.-H. Hsu, P. Stano, Y. Sato, S. Matsuo, S. Tarucha, and D. Loss, Charge transport of a spin-orbit-coupled Luttinger liquid, *Phys. Rev. B* **100**, 195423 (2019).
- [123] C. L. Kane and M. P. A. Fisher, Nonequilibrium noise and fractional charge in the quantum Hall effect, *Phys. Rev. Lett.* **72**, 724 (1994).
- [124] L. Saminadayar, D. C. Glattli, Y. Jin, and B. Etienne, Observation of the $e/3$ Fractionally Charged Laughlin Quasiparticle, *Phys. Rev. Lett.* **79**, 2526 (1997).
- [125] R. de Picciotto, M. Reznikov, M. Heiblum, V. Umansky, G. Bunin, and D. Mahalu, Direct observation of a fractional charge, *Nature* **389**, 162 (1997).
- [126] C. R. Dean, L. Wang, P. Maher, C. Forsythe, F. Ghahari, Y. Gao, J. Katoch, M. Ishigami, P. Moon, M. Koshino, T. Taniguchi, K. Watanabe, K. L. Shepard, J. Hone, and P. Kim, Hofstadter's butterfly and the fractal quantum Hall effect in moiré superlattices, *Nature* **497**, 598 (2013).
- [127] B. Hunt, J. D. Sanchez-Yamagishi, A. F. Young, M. Yankowitz, B. J. LeRoy, K. Watanabe, T. Taniguchi, P. Moon, M. Koshino, P. Jarillo-Herrero, and R. C. Ashoori, Massive Dirac Fermions and Hofstadter Butterfly in a van der Waals Heterostructure, *Science* **340**, 1427 (2013).
- [128] L. A. Ponomarenko, R. V. Gorbachev, G. L. Yu, D. C. Elias, R. Jalil, A. A. Patel, A. Mishchenko, A. S. Mayorov, C. R. Woods, J. R. Wallbank, M. Mucha-Kruczynski, B. A. Piot, M. Potemski, I. V. Grigorieva, K. S. Novoselov, F. Guinea, V. I. Fal'ko, and A. K. Geim, Cloning of Dirac fermions in graphene superlattices, *Nature* **497**, 594 (2013).
- [129] P. Moon and M. Koshino, Electronic properties of graphene/hexagonal-boron-nitride moiré superlattice, *Phys. Rev. B* **90**, 155406 (2014).
- [130] H. Kim, N. Leconte, B. L. Chittari, K. Watanabe, T. Taniguchi, A. H. MacDonald, J. Jung, and S. Jung, Accurate Gap Determination in Monolayer and Bilayer Graphene/h-BN Moiré Superlattices, *Nano Lett.* **18**, 7732 (2018).
- [131] M. Kindermann, B. Uchoa, and D. L. Miller, Zero-energy modes and gate-tunable gap in graphene on hexagonal boron nitride, *Phys. Rev. B* **86**, 115415 (2012).
- [132] P. Fendley, Parafermionic edge zero modes in Z_n -invariant spin chains, *J. Stat. Mech.* **2012**, P11020 (2012).
- [133] D. J. Clarke, J. Alicea, and K. Shtengel, Exotic non-Abelian anyons from conventional fractional quantum Hall states, *Nat. Commun.* **4**, 1348 (2013).
- [134] J. Klinovaja, A. Yacoby, and D. Loss, Kramers pairs of Majorana fermions and parafermions in fractional topological insulators, *Phys. Rev. B* **90**, 155447 (2014).
- [135] R. S. K. Mong, D. J. Clarke, J. Alicea, N. H. Lindner, P. Fendley, C. Nayak, Y. Oreg, A. Stern, E. Berg, K. Shtengel, and M. P. A. Fisher, Universal Topological Quantum Computation from a Superconductor-Abelian Quantum Hall Heterostructure, *Phys. Rev. X* **4**, 011036 (2014).
- [136] T. Meng and E. Sela, Time reversal symmetry broken fractional topological phases at zero magnetic field, *Phys. Rev. B* **90**, 235425 (2014).
- [137] Y. Oreg, E. Sela, and A. Stern, Fractional helical liquids in quantum wires, *Phys. Rev. B* **89**, 115402 (2014).
- [138] E. Sagi, Y. Oreg, A. Stern, and B. I. Halperin, Imprint of topological degeneracy in quasi-one-dimensional fractional quantum Hall states, *Phys. Rev. B* **91**, 245144 (2015).
- [139] E. Sagi, A. Haim, E. Berg, F. von Oppen, and Y. Oreg, Fractional chiral superconductors, *Phys. Rev. B* **96**, 235144 (2017).
- [140] K. Laubscher, D. Loss, and J. Klinovaja, Fractional topological superconductivity and parafermion corner states, *Phys. Rev. Research* **1**, 032017(R) (2019).
- [141] K. Laubscher, D. Loss, and J. Klinovaja, Majorana and parafermion corner states from two coupled sheets of bilayer graphene, *Phys. Rev. Research* **2**, 013330 (2020).
- [142] C. Zhang, C.-P. Chuu, X. Ren, M.-Y. Li, L.-J. Li, C. Jin, M.-Y. Chou, and C.-K. Shih, Interlayer couplings, Moiré patterns, and 2D electronic superlattices in $\text{MoS}_2/\text{WSe}_2$ hetero-bilayers, *Sci. Adv.* **3**, e1601459 (2017).
- [143] Z.-D. Song and B. A. Bernevig, Magic-Angle Twisted Bilayer Graphene as a Topological Heavy Fermion Problem, *Phys. Rev. Lett.* **129**, 047601 (2022).
- [144] H. Shi and X. Dai, Heavy-fermion representation for twisted

- bilayer graphene systems, Phys. Rev. B **106**, 245129 (2022).
- [145] L. L. H. Lau and P. Coleman, Topological Mixed Valence Model for Twisted Bilayer Graphene, (2023), arXiv:2303.02670 [cond-mat.str-el].
- [146] P. Lecheminant, A. O. Gogolin, and A. A. Nersesyan, Criticality in self-dual sine-Gordon models, Nucl. Phys. B **639**, 502 (2002).
- [147] F. Ronetti, D. Loss, and J. Klinovaja, Clock model and parafermions in Rashba nanowires, Phys. Rev. B **103**, 235410 (2021)

Supplemental Material to “General scatterings and electronic states in the quantum-wire network of moiré systems”

Chen-Hsuan Hsu^{1,2,3}, Daniel Loss^{3,4}, and Jelena Klinovaja⁴

¹*Yukawa Institute for Theoretical Physics, Kyoto University, Kyoto 606-8502, Japan*

²*Institute of Physics, Academia Sinica, Taipei 115, Taiwan*

³*RIKEN Center for Emergent Matter Science, Wako, Saitama 351-0198, Japan*

⁴*Department of Physics, University of Basel, Klingelbergstrasse 82, CH-4056 Basel, Switzerland*

I. Conventional scatterings

In this section we discuss conventional scatterings, which fulfill Eq. (7) in the main text and can take place at any fillings. This category includes charge-density-wave (CDW) couplings, Josephson couplings, and hoppings, corresponding to the “crystalline states” discussed in spinless fermion systems [S1].

We start with the generalized CDW couplings, which include higher-order processes involving a single wire or multiple wires. For simplicity, we focus on processes with $\bar{S}_{p,c} = 0$ for any p . It allows us to rewrite the coefficients $s_{\ell p\sigma}$ with integers $N_{p\sigma}$,

$$(s_{Rp\uparrow}, s_{Lp\uparrow}, s_{Rp\downarrow}, s_{Lp\downarrow}) = (-N_{p\uparrow}, N_{p\uparrow}, -N_{p\downarrow}, N_{p\downarrow}), \quad (\text{S1})$$

which fulfill the global particle number conservation. Furthermore, the integer set fulfills the momentum conservation when $\sum_p (N_{p\uparrow} + N_{p\downarrow}) = 0$. The operator can be bosonized in the form of Eq. (9) in the main text with $S_{p,\xi} = 2(N_{p\uparrow} + \xi N_{p\downarrow})$ and $\bar{S}_{p,\xi} = 0$. As an example, in Fig. S1(a) we illustrate the two-wire scattering process with $(N_{0\uparrow}, N_{0\downarrow}, N_{n\uparrow}, N_{n\downarrow}) = (-1, -1, 1, 1)$ and $N_{p\sigma} = 0$ for $p \neq 0, n$. It is straightforward to check that, for sufficiently strong electron-electron interaction, the CDW operator is RG relevant, leading to the CDW phase with an insulating bulk.

In addition, the generalized Josephson couplings (assuming singlet pairing) can be characterized by integers M_p and N_p ,

$$(s_{Rp\uparrow}, s_{Lp\uparrow}, s_{Rp\downarrow}, s_{Lp\downarrow}) = (-M_p, N_p, N_p, -M_p), \quad (\text{S2})$$

which already incorporates the momentum conservation condition. Moreover, the global particle number conservation is ensured by $\sum_p (N_p - M_p) = 0$. The operator can be bosonized in the form of Eq. (9) in the main text with $\bar{S}_{p,c} = 2(N_p - M_p)$, $S_{p,s} = 2(N_p + M_p)$, $S_{p,c} = 0$, and $\bar{S}_{p,s} = 0$. When the corresponding operator is RG relevant, the system is in the superconducting state. An example with $(N_0, M_0, N_n, M_n) = (0, -1, 0, 1)$ and $N_p, M_p = 0$ for $p \neq 0, n$. is illustrated in Fig. S1(b).

There are also generalized hopping processes, including single-particle hopping and pair hopping between wires. In contrast to the above, the expression for this type of scatterings cannot be simplified; we therefore keep the general notation $s_{\ell p\sigma}$ in Eq. (3). If the operator is RG relevant, it can lead to a two-dimensional Fermi liquid [S2–S5]. An example with $(s_{R0\sigma}, s_{Rn\sigma}, s_{L0\sigma}, s_{Ln\sigma}) = (-1, 1, 0, 0)$ is illustrated in Fig. S1(c).

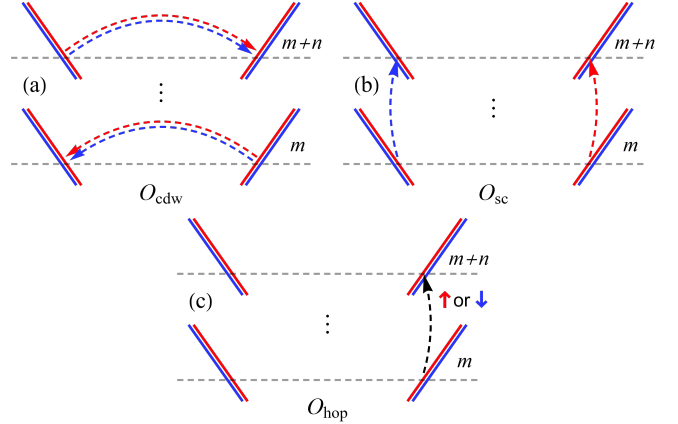


FIG. S1. Illustrations of conventional scattering processes, which can take place at any fillings. (a) CDW coupling, characterized by Eq. (S1) with $(N_{0\uparrow}, N_{0\downarrow}, N_{n\uparrow}, N_{n\downarrow}) = (-1, -1, 1, 1)$. (b) Josephson coupling, characterized by Eq. (S2) with $(N_0, M_0, N_n, M_n) = (0, -1, 0, 1)$. (c) Single-particle hopping, characterized by Eq. (3) with $(s_{R0\sigma}, s_{Rn\sigma}, s_{L0\sigma}, s_{Ln\sigma}) = (-1, 1, 0, 0)$ for $\sigma = \uparrow$ or \downarrow .

II. Moiré umklapp scatterings

In this section, we summarize the four types of moiré umklapp scatterings, before discussing the scattering described by O_{iv} in more detail. Aiming at a systematic construction of the scattering operators, for each of the types we will introduce positive integer coefficients, in order to decrease the number of independent coefficients. We start with processes involving only single wires and denote the corresponding operator as O_i . In the form of Eq. (3), O_i is characterized by the following nonzero $s_{\ell p\sigma}$,

$$(s_{R0\sigma}, s_{L0\sigma}) = (N_\sigma, -N_\sigma), \quad (\text{S3})$$

with positive integers N_σ .

Next, there are umklapp processes involving multiple wires with correlated intrawire scatterings. The simplest case involves two n -th nearest neighboring wires, labeled as O_{ii} , with nonzero $s_{\ell p\sigma}$,

$$(s_{R0\sigma}, s_{L0\sigma}, s_{Rn\sigma}, s_{Ln\sigma}) = (N_{0\sigma}, -N_{0\sigma}, N_{n\sigma}, -N_{n\sigma}), \quad (\text{S4})$$

with positive integers $N_{0\sigma}$ and $N_{n\sigma}$.

Furthermore, we consider moiré umklapp scatterings with interwire processes while still conserving the particle number for each wire. The latter condition implies $\bar{S}_{p,c} = 0$ for any

TABLE S1. Moiré umklapp scatterings. The operators, O_i – O_{iv} , are in the fermion form in Eq. (3) with the listed $s_{\ell p \sigma}$ values and \mathbb{N} denoting the positive integer set. The scatterings are allowed at the listed filling factor ν , with P being a nonzero integer. The bosonized form is in Eq. (9) with the listed $S_{p,\xi}$ and $\bar{S}_{p,\xi}$ values. While we list two-wire processes for O_{ii} – O_{iv} for simplicity, processes involving more wires are generally allowed as long as Eqs. (4)–(5) are fulfilled.

Operator	$s_{\ell p \sigma}$	possible values	ν	$S_{p,\xi}$	$\bar{S}_{p,\xi}$
O_i	$\ell \delta_{p0} N_\sigma$	$N_\sigma \in \mathbb{N}$	$\frac{P}{\sum_\sigma N_\sigma}$	$-2\delta_{p0}(N_\uparrow + \xi N_\downarrow)$	0
O_{ii}	$\ell(\delta_{p0} + \delta_{pn}) N_{p\sigma}$	$N_{0\sigma}, N_{n\sigma} \in \mathbb{N}$	$\frac{P}{\sum_\sigma (N_{0\sigma} + N_{n\sigma})}$	$-2(\delta_{p0} + \delta_{pn})(N_\uparrow + \xi N_\downarrow)$	0
O_{iii}	$\ell(\delta_{p0} + \delta_{pn}) N_\sigma$	$N_\sigma \in \mathbb{N}$	$\frac{P}{2 \sum_\sigma N_\sigma}$	$-2(\delta_{p0} + \delta_{pn})(N_\uparrow + \xi N_\downarrow)$	0
O_{iv}	$\delta_{\ell R}(\delta_{p0} N_\sigma + \delta_{pn} M_\sigma)$ $-\delta_{\ell L}(\delta_{p0} M_\sigma + \delta_{pn} N_\sigma)$	$N_\sigma, M_\sigma \in \mathbb{N}, N_\sigma \neq M_\sigma$	$\frac{P}{\sum_\sigma (N_\sigma + M_\sigma)}$	$-2(\delta_{p0} + \delta_{pn})\delta_{\xi c}(N_\uparrow + M_\downarrow)$ $-2(\delta_{p0} + \delta_{pn})\delta_{\xi s}(N_\uparrow - N_\downarrow)$	$2(\delta_{p0} - \delta_{pn})\delta_{\xi c}(N_\uparrow - M_\uparrow)$

p . Together with the choice $\bar{S}_{p,s} = 0$ and limiting ourselves to processes involving two n -th nearest neighboring wires, we get O_{iii} with nonzero $s_{\ell p \sigma}$ given by

$$(s_{R0\sigma}, s_{L0\sigma}, s_{Rn\sigma}, s_{Ln\sigma}) = (N_\sigma, -N_\sigma, N_\sigma, -N_\sigma), \quad (S5)$$

with positive integers N_σ .

Finally, allowing for processes which do not conserve the particle number for some wires, we have $\bar{S}_{p,c} \neq 0$ for some p . Taking two-wire processes for simplicity and $\bar{S}_{p,s} = 0$, we have O_{iv} as Eq. (3) with

$$(s_{R0\sigma}, s_{L0\sigma}, s_{Rn\sigma}, s_{Ln\sigma}) = (N_\sigma, -M_\sigma, M_\sigma, -N_\sigma), \quad (S6)$$

with positive integers N_σ and M_σ . Here $N_\sigma \neq M_\sigma$, as otherwise we would have processes already included in O_{iii} . By introducing indices such as N_σ and M_σ , we can decrease the number of independent indices within a scattering subtype, enabling a systematic construction of the scattering operators. We summarize the moiré umklapp scatterings in Table S1, which includes higher-order processes for general filling factors.

Owing to their possibility for hosting chiral edge modes, we analyze the moiré umklapp scattering described by O_{iv} in more detail. As in the main text, we have

$$H_{iv} = \sum_m g_{iv} \int dx \cos(\sqrt{2}S_{0,c}\tilde{\Phi}_{m,n}), \quad (S7)$$

with the coupling parameter g_{iv} and the transformed field $\tilde{\Phi}_{m,n}$ introduced in the main text. Here, we have further simplified our analysis by considering processes with $N_\uparrow = N_\downarrow$, i.e., $S_{p,s} = 0$. With the coefficients in Eq. (S6), we have $S_{0,c} = -(N_\uparrow + N_\downarrow + M_\uparrow + M_\downarrow)$ and $f = (N_\uparrow - M_\uparrow)/(N_\uparrow + M_\downarrow)$. Using the commutator in Eq. (11), it can be shown that the transformed field fulfills the relation,

$$\begin{aligned} [\tilde{\Phi}_{m,n}(x), \tilde{\Phi}_{m',n}(x')] &= \frac{1}{4} \left([\Phi_{L,m+n}(x), \Phi_{L,m'+n}(x')] \right. \\ &\quad \left. + [\Phi_{R,m}(x), \Phi_{R,m'}(x')] \right) \\ &= (-1 + 1) \frac{\pi i f}{4} \delta_{mm'} \text{sign}(x - x') \\ &= 0. \end{aligned} \quad (S8)$$

Since the $\tilde{\Phi}_{m,n}$ fields for all m commute with each other, the cosine terms in Eq. (S7) can be ordered simultaneously, gapping out the bulk modes. Introducing $\tilde{\Theta}_{m,n} = (\Phi_{L(m+n)} + \Phi_{Rm})/2$, we obtain the additional relations,

$$\begin{aligned} [\tilde{\Theta}_{m,n}(x), \tilde{\Theta}_{m',n}(x')] &= 0, \\ [\tilde{\Phi}_{m,n}(x), \tilde{\Theta}_{m',n}(x')] &= \frac{i\pi}{2} f \delta_{mm'} \text{sign}(x' - x). \end{aligned} \quad (S9)$$

To proceed, we follow Kane et al. [S1] and express the forward-scattering term of the density-density interaction in the transformed basis, where the unperturbed part of the effective action is given by

$$\begin{aligned} \frac{\tilde{S}_0}{\hbar} &= \sum_m \int \frac{dx d\tau}{\pi} \left[\frac{-i}{f} (\partial_x \tilde{\Theta}_{m,n})(\partial_\tau \tilde{\Phi}_{m,n}) \right. \\ &\quad \left. + \left(\frac{v_0}{2} + \frac{U}{\hbar} \right) \left(\partial_x \tilde{\Phi}_{m,n} \right)^2 + \frac{v_0}{2} \left(\partial_x \tilde{\Theta}_{m,n} \right)^2 \right]. \end{aligned} \quad (S10)$$

We note that the fraction f comes from the above commutator and will enter the scaling dimensions of various operators containing $\tilde{\Phi}_{m,n}$ or $\tilde{\Theta}_{m,n}$. In the momentum and Matsubara frequency domain, we have

$$\begin{aligned} \frac{\tilde{S}_0}{\hbar} &= \frac{1}{2\pi\beta\hbar\Omega} \sum_m \sum_{q,\omega_n} \left(\tilde{\Phi}_{m,n}^*(q, \omega_n), \tilde{\Theta}_{m,n}^*(q, \omega_n) \right) \\ &\quad \times \begin{pmatrix} v_0 q^2 (1 + \frac{2U}{\hbar v_0}) & \frac{i}{f} q \omega_n \\ \frac{i}{f} q \omega_n & v_0 q^2 \end{pmatrix} \begin{pmatrix} \tilde{\Phi}_{m,n}(q, \omega_n) \\ \tilde{\Theta}_{m,n}(q, \omega_n) \end{pmatrix}. \end{aligned} \quad (S11)$$

Inverting the matrix above, one can compute $\langle [\tilde{\Phi}_{m,n}(x, \tau) - \tilde{\Phi}_{m,n}(0, 0)]^2 \rangle$ with respect to \tilde{S}_0 and obtain the scaling dimension of O_{iv} ,

$$\Delta_{iv} = \frac{1}{2} |f| S_{0,c}^2 \left(1 + \frac{2U}{\hbar v_0} \right)^{-1/2}, \quad (S12)$$

which gives Eq. (13) in the main text. Taking the coefficients in Eq. (S6), one obtains

$$\Delta_{iv} = 2(N_\uparrow + M_\downarrow) |N_\uparrow - M_\uparrow| \left(1 + \frac{2U}{\hbar v_0} \right)^{-\frac{1}{2}}. \quad (S13)$$

In consequence, for a given set of (N_σ, M_σ) , the scaling dimension Δ_{iv} can be below 2 for sufficiently large U .

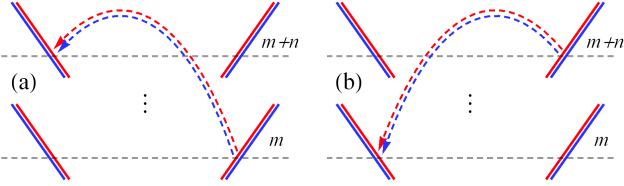


FIG. S2. O_{iv} processes of the moiré umklapp scatterings at half filling, described by (a) O_a in Eq. (S14) and (b) O_b in Eq. (S15).

III. Chirality domains

In this section we discuss the O_{iv} processes of the moiré umklapp scatterings and the formation of chirality domains. For concreteness, we consider the two processes allowed at half filling in Fig. S2; the following discussion can be straightforwardly generalized to other fillings. The process in Fig. S2(a) is described by

$$O_a = \sum_{m=1} \psi_{L(m+n)\uparrow}^\dagger \psi_{Rm\uparrow} \psi_{L(m+n)\downarrow}^\dagger \psi_{Rm\downarrow}, \quad (\text{S14})$$

corresponding to O_{iv} with $N_\uparrow = N_\downarrow = 1$ and $M_\uparrow = M_\downarrow = 0$ [see Eq. (S6)]. The process in Fig. S2(b) is

$$O_b = \sum_{m=1} \psi_{Lm\uparrow}^\dagger \psi_{R(m+n)\uparrow} \psi_{Lm\downarrow}^\dagger \psi_{R(m+n)\downarrow}, \quad (\text{S15})$$

corresponding to $N_\uparrow = N_\downarrow = 0$ and $M_\uparrow = M_\downarrow = 1$. At the half filling, both O_a and O_b preserve the particle number, spin, and momentum conservation, and therefore fulfill Eqs. (4)–(5) in the main text.

Next, we discuss the stability of the chiral edge modes. Consider the following operators in the bosonized form,

$$O_a + O_a^\dagger \propto \sum_{m=1} \cos \left\{ \sqrt{2} [\Phi_{L(m+n)} - \Phi_{Rm}] \right\}, \quad (\text{S16a})$$

$$O_b + O_b^\dagger \propto \sum_{m=1} \cos \left\{ \sqrt{2} [\Phi_{R(m+n)} - \Phi_{Lm}] \right\}, \quad (\text{S16b})$$

where we have a $\leftrightarrow b$ upon swapping R and L . If we are in the parameter regime given in Eq. (13) in the main text, where the operators $O_{a,b}$ are RG relevant, their coupling constants can flow to the strong-coupling limit, leading to correlated states with the opposite chirality of the edge modes.

One may wonder if we have the following perturbation,

$$\delta H = \int dx (g_a O_a + g_b O_b + \text{H.c.}), \quad (\text{S17})$$

whether the edge modes created by a cosine term in δH would be gapped out by the other, resulting in a fully gapped system. However, it can be shown that the operators do not commute,

$$[O_a(x) + O_a^\dagger(x), O_b(x') + O_b^\dagger(x')] \neq 0, \quad (\text{S18})$$

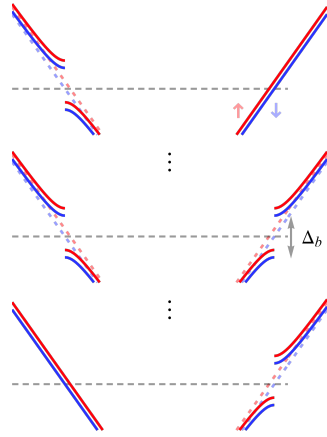


FIG. S3. The moiré umklapp scattering O_{iv} induces a bulk gap Δ_b opening in the interior of the system while leaving chiral edge modes gapless. The gap opening around the Fermi point $\pm k_F$ leads to a lowering of the energy bands (solid curves) compared to those before the gap opening (dotted curves). This results in an energy gain $\delta\epsilon_q$ at momentum $\hbar q$ and the total energy gain per branch given by Eq. (S20).

so they cannot be ordered simultaneously. Therefore, even if O_a and O_b coexist in δH and are both RG relevant, only one of them can open a bulk gap, as shown in Fig. S3.

In each gapped branch, there is an energy gain at momentum $\hbar q$ [S6],

$$\delta\epsilon_q = \frac{\epsilon_q - \epsilon_{q'}}{2} + \sqrt{\left(\frac{\epsilon_q - \epsilon_{q'}}{2}\right)^2 + \Delta_b^2}, \quad (\text{S19})$$

with the dispersion $\epsilon_q = \hbar v_0 |q|$, $q' = q - 2k_F$ for $q \in [0, k_F]$, $q' = q + 2k_F$ for $q \in [-k_F, 0]$, and the (renormalized) bulk gap Δ_b . The Peierls energy gain per branch can be obtained by an integral over momentum,

$$\frac{L}{2\pi} \int_0^{k_F} dq \delta\epsilon_q \approx \frac{k_F L}{2\pi} \frac{\Delta_b^2}{\hbar v_0 k_F} \ln \left| \frac{2\hbar v_0 k_F}{\Delta_b} \right|, \quad (\text{S20})$$

where we have kept the leading order in $\Delta_b/(\hbar v_0 k_F)$. Consequently, the bulk gap opening results in a Peierls energy gain. It is therefore energetically favorable that the system evolves from the crossed sliding Luttinger liquid to the moiré correlated state to open a gap at sufficiently low temperature.

In consequence, whereas the Hamiltonian may allow for the formation of both chirality states, we expect that the system undergoes spontaneous symmetry breaking. At the transition, an infinitesimal perturbation will select one of the chirality states within a domain. This situation is analogous to the Ising ferromagnetic phase. While the ground state can have positive or negative magnetization, only one of them will be stabilized within a magnetic domain as the temperature is lowered through the transition from the paramagnetic to the ferromagnetic phase. As a result, we expect the formation of chirality domains in the moiré correlated state. While the domain walls cost energy, it is generally anticipated that domains can

form, contributing to an increase in entropy and consequently a decrease in free energy at finite temperatures. Given that a chirality domain can carry finite orbital magnetization and couple to magnetic moments, we postulate that local magnetic moments (potentially induced by disorder) can initiate the formation of these domains. Remarkably, in Refs. [S7, S8], the stabilization of a definite chirality state in micrometer-sized systems requires a finite magnetic field to train domains in the samples.

It is worth mentioning that an alternative scenario is possible where the perturbation in Eq. (S17) realizes a self-dual sine-Gordon model [S9]. While this leads to an intriguing possibility for stabilizing parafermion modes without superconductivity [S10], the detailed analysis of the self-dual sine-Gordon model is beyond the scope of this work.

IV. Experimental features for the edge modes

In this section we discuss the experimental features for the edge modes when the system is in one of the moiré correlated states with a gapped bulk and gapless edges. For simplicity we consider here Eq. (S6) with $N_\uparrow = N_\downarrow = M + 1$, $M_\uparrow = M_\downarrow = M$, $n = 1$, and a single domain in the system. This choice allows us to focus on a simpler case in which a single mode appears at one edge and to construct the effective edge theory from the commutator, given in Eq. (11) in the main text [S11–S13],

$$\frac{S_{\text{edge}}}{\hbar} = \int \frac{dx d\tau}{4\pi f} \left[-i\partial_x \phi \partial_\tau \phi + v_{\text{edge}} (\partial_x \phi)^2 \right], \quad (\text{S21})$$

where ϕ is the chiral boson field satisfying $[\phi(x), \phi(x')] = i\pi f \text{sign}(x - x')$ at the edge and v_{edge} its velocity.

The local density of states is given by [S12, S14]

$$\rho(\epsilon) = \frac{1}{\pi} \text{Re} \left[\int_0^\infty dt e^{i\epsilon t/\hbar} \langle \psi_e(t) \psi_e^\dagger(0) \rangle \right], \quad (\text{S22})$$

where $\psi_e = e^{i\phi/f}$ denotes the excitation operator with a unit charge. Computing the average in $\langle \dots \rangle$ with respect to the action S_{edge} and performing the time integral, one gets the local density of states, which follows the universal scaling curve Eq. (14) given in the main text and reduces to a power law $\rho(\epsilon) \propto |\epsilon|^{1/f-1}$ as $T \rightarrow 0$. The scaling behavior in the spectroscopic features can be verified through scanning tunneling spectroscopy, as earlier studies on carbon nanotubes [S15].

Next, we discuss the transport features of the edge modes in the settings illustrated in Fig. 4 in the main text. The setting in Fig. 4(a) allows for an interedge tunneling process, which can be described as

$$S_t = t_0 \int d\tau e^{i(\phi_1 - \phi_2)/f}, \quad (\text{S23})$$

with the tunnel amplitude t_0 . In the above, we include a subscript in the ϕ field to label the two edges. One can derive the

RG flow equation for the tunnel amplitude,

$$\frac{d\tilde{t}_0}{dl} = \left(1 - \frac{1}{f}\right) \tilde{t}_0, \quad (\text{S24})$$

where $\tilde{t}_0 = t_0/\Delta_a$ is the dimensionless coupling with the high-energy cutoff $\Delta_a = \hbar v_{\text{edge}}/a$ and the dimensionless length scale l . By integrating the RG flow equation up to the scale l^* corresponding to the high-bias (V) or high-temperature (T) regime, one gets the renormalized coupling and differential tunneling conductance,

$$\frac{dI_t}{dV} \propto \tilde{t}_0^2(l^*) \propto \max(eV, k_B T)^{\frac{2}{f}-2}. \quad (\text{S25})$$

Alternatively, one can directly compute the current through a tunneling barrier separating two Luttinger liquids [S16] and obtain a universal scaling formula for general V and T given in Eq. (15) in the main text.

On the other hand, the QPC setting in Fig. 4(b) leads to an interedge backscattering process,

$$S_b = v_b \int d\tau e^{i(\phi_1 - \phi_2)}. \quad (\text{S26})$$

The RG flow equation for the backscattering strength v_b is

$$\frac{d\tilde{v}_b}{dl} = (1 - f) \tilde{v}_b, \quad (\text{S27})$$

with $\tilde{v}_b = v_b/\Delta_a$. It leads to a backscattering current in the opposite edge and therefore a correction $\delta G < 0$ in the edge (differential) conductance with the magnitude,

$$|\delta G| \propto \tilde{v}_b^2(l^*) \propto \max(eV, k_B T)^{2f-2}. \quad (\text{S28})$$

Crucially, as long as the operator O_{iv} is RG relevant, the scaling exponents do not depend on the details of the fixed-point Hamiltonian $H_0 + H_{\text{fs}}$, a feature similar to edge transport of the fractional quantum Hall states [S11–S13]; we therefore do not explicitly give the form of $H_0 + H_{\text{fs}}$ in the main text. As a note, for a general set of $(N_\uparrow, N_\downarrow, M_\uparrow, M_\downarrow)$ and n , there can be multiple gapless modes at an edge, and the forward scattering between the edge modes can lead to nonuniversal exponents [S17, S18].

V. Unperturbed Hamiltonian

In this section we discuss a specific model describing the crossed sliding (Tomonaga-)Luttinger Liquid fixed point. In

the literature [S2–S5], the following model was adopted,

$$\begin{aligned} H_0 + H_{\text{fs}} &= \sum_{j=1}^3 H_c^{(j)} + \sum_{j=1}^3 H_s^{(j)}, \\ H_c^{(j)} &= \sum_{mm'} \int \frac{\hbar dx}{2\pi} \left[V_{\phi,mm'}^j (\partial_x \phi_{cm}^j) (\partial_x \phi_{cm'}^j) \right. \\ &\quad \left. + V_{\theta,mm'}^j (\partial_x \theta_{cm}^j) (\partial_x \theta_{cm'}^j) \right], \\ H_s^{(j)} &= \sum_m \int \frac{\hbar dx}{2\pi} \left[\frac{u_s}{K_s} (\partial_x \phi_{sm}^j)^2 + u_s K_s (\partial_x \theta_{sm}^j)^2 \right], \end{aligned} \quad (\text{S29a})$$

which has been modified for the TBG problem [S19]. For each array labeled by j , we separate the charge $H_c^{(j)}$ and spin $H_s^{(j)}$ sectors. The spin sector is characterized by the velocity u_s and the interaction parameter K_s , set to be identical for all the wires. The charge sector contains the intrawire and interwire terms of the density-density V_ϕ^j and current-current V_θ^j interactions and can be Fourier transformed,

$$\begin{aligned} H_c^{(j)} &= \frac{1}{\Omega_\perp} \sum_{q_\perp} \int \frac{\hbar dx}{2\pi} \left[\frac{u_c^j(q_\perp)}{K_c^j(q_\perp)} \left| \partial_x \phi_c^j(q_\perp) \right|^2 \right. \\ &\quad \left. + u_c^j(q_\perp) K_c^j(q_\perp) \left| \partial_x \theta_c^j(q_\perp) \right|^2 \right], \end{aligned} \quad (\text{S29b})$$

with the momentum q_\perp in the perpendicular direction to the wire (that is, $\perp x$) and $\Omega_\perp = N_\perp d$. Here, the velocity u_c^j and the interaction function K_c^j (a generalization of the interaction parameter) are functions of q_\perp ,

$$u_c^j(q_\perp) \equiv \sqrt{V_\phi^j(q_\perp) V_\theta^j(q_\perp)}, \quad (\text{S30a})$$

$$K_c^j(q_\perp) \equiv \sqrt{V_\theta^j(q_\perp) / V_\phi^j(q_\perp)}. \quad (\text{S30b})$$

For a system with the periodic boundary condition perpendicular to the wire (that is, parallel to q_\perp), it would be natural to express V_ϕ^j and V_θ^j as periodic functions of q_\perp . Nonetheless, existing works took (the inverse of) the interaction function as a Fourier series of q_\perp [S2–S5, S19],

$$\frac{1}{K_c(q_\perp)} = \sum_{m=0}^{\infty} \kappa_m \cos(mq_\perp d), \quad (\text{S31})$$

identical for all j here. This choice makes it possible to express the scaling dimensions using the following dimensionless parameters,

$$\Delta_{\phi n} = \int_{-\pi}^{\pi} \frac{d(q_\perp d)}{2\pi} K_c(q_\perp) \cos(nq_\perp d), \quad (\text{S32a})$$

$$\Delta_{\theta n} = \int_{-\pi}^{\pi} \frac{d(q_\perp d)}{2\pi} \frac{\cos(nq_\perp d)}{K_c(q_\perp)}. \quad (\text{S32b})$$

We note that neglecting the marginally relevant interwire forward scattering terms amounts to truncate Eq. (S31) at $m = 0$.

In Ref. [S2], the series was truncated at $m = 1$. In Refs. [S3–S5, S19], the authors kept terms up to $m = 2$, leading to

$$\frac{1}{K_c(q_\perp)} = \frac{1}{K_{c0}} [1 + \lambda_1 \cos(q_\perp d) + \lambda_2 \cos(2q_\perp d)]. \quad (\text{S33})$$

As discussed here, the choice of Eqs. (S29)–(S31) is not general. Therefore, instead of limiting our discussions to a particular model, we keep a general form for $H_0 + H_{\text{fs}}$ in the main text. We note that, with this specific model, one can obtain a power-law T dependence of the resistivity, as predicted in earlier works on similar models [S2, S4, S5].

For the specific model listed in Eqs. (S29)–(S31), we compute the scaling dimension of the general scattering operator $O_{\{s_{\ell p \sigma}\}}$ given in Eq. (9) in the main text,

$$\begin{aligned} \Delta_{\{s_{\ell p \sigma}\}} &= \frac{1}{8} \sum_{p,p'} [S_{p,c} S_{p',c} \Delta_{\phi(p-p')} + \bar{S}_{p,c} \bar{S}_{p',c} \Delta_{\theta(p-p')}] \\ &\quad + \frac{1}{8} \sum_p [S_{p,s}^2 K_s + \frac{\bar{S}_{p,s}^2}{K_s}], \end{aligned} \quad (\text{S34})$$

with the coefficients

$$S_{p,c} = s_{Lp\uparrow} - s_{Rp\uparrow} + s_{Lp\downarrow} - s_{Rp\downarrow}, \quad (\text{S35a})$$

$$\bar{S}_{p,c} = s_{Lp\uparrow} + s_{Rp\uparrow} + s_{Lp\downarrow} + s_{Rp\downarrow}, \quad (\text{S35b})$$

$$S_{p,s} = s_{Lp\uparrow} - s_{Rp\uparrow} - s_{Lp\downarrow} + s_{Rp\downarrow}, \quad (\text{S35c})$$

$$\bar{S}_{p,s} = s_{Lp\uparrow} + s_{Rp\uparrow} - s_{Lp\downarrow} - s_{Rp\downarrow}. \quad (\text{S35d})$$

When the interaction function $K_c(q_\perp)$ is specified, such as the one in Eq. (S33), the integrals in Eq. (S32) can be computed directly.

For scattering processes within an array, the RG relevance for the corresponding operators is determined by

$$\Delta_{\{s_{\ell p \sigma}\}} < 2, \quad (\text{S36})$$

where the right-hand side comes from the temporal and spatial integrals in the action [S20]. When the operator $O_{\{s_{\ell p \sigma}\}}$ is RG relevant, the crossed sliding Luttinger liquid is unstable against the perturbation, leading to an electronic state characterized by $O_{\{s_{\ell p \sigma}\}}$. For interarray scattering processes, which take place at wire intersections, on the other hand, the RG relevance condition becomes $\Delta_{\{s_{\ell p \sigma}\}} < 1$, owing to the lack of the spatial integral in the action. Therefore, the RG relevance condition is stricter than those within an array; we therefore examine the scatterings within an array in more detail throughout the main text.

[S1] C. L. Kane, R. Mukhopadhyay, and T. C. Lubensky, Fractional Quantum Hall Effect in an Array of Quantum Wires, Phys. Rev. Lett. **88**, 036401 (2002).

[S2] V. J. Emery, E. Fradkin, S. A. Kivelson, and T. C. Lubensky, Quantum Theory of the Smectic Metal State in Stripe Phases, Phys. Rev. Lett. **85**, 2160 (2000).

- [S3] A. Vishwanath and D. Carpentier, Two-Dimensional Anisotropic Non-Fermi-Liquid Phase of Coupled Luttinger Liquids, *Phys. Rev. Lett.* **86**, 676 (2001).
- [S4] R. Mukhopadhyay, C. L. Kane, and T. C. Lubensky, Crossed sliding Luttinger liquid phase, *Phys. Rev. B* **63**, 081103 (2001).
- [S5] R. Mukhopadhyay, C. L. Kane, and T. C. Lubensky, Sliding Luttinger liquid phases, *Phys. Rev. B* **64**, 045120 (2001).
- [S6] T. Meng, P. Stano, J. Klinovaja, and D. Loss, Helical nuclear spin order in a strip of stripes in the quantum Hall regime, *Eur. Phys. J. B* **87**, 203 (2014).
- [S7] A. L. Sharpe, E. J. Fox, A. W. Barnard, J. Finney, K. Watanabe, T. Taniguchi, M. A. Kastner, and D. Goldhaber-Gordon, Emergent ferromagnetism near three-quarters filling in twisted bilayer graphene, *Science* **365**, 605 (2019).
- [S8] M. Serlin, C. L. Tschirhart, H. Polshyn, Y. Zhang, J. Zhu, K. Watanabe, T. Taniguchi, L. Balents, and A. F. Young, Intrinsic quantized anomalous Hall effect in a moiré heterostructure, *Science* **367**, 900 (2020).
- [S9] P. Lecheminant, A. O. Gogolin, and A. A. Nersesyan, Criticality in self-dual sine-Gordon models, *Nucl. Phys. B* **639**, 502 (2002).
- [S10] F. Ronetti, D. Loss, and J. Klinovaja, Clock model and parafermions in Rashba nanowires, *Phys. Rev. B* **103**, 235410 (2021).
- [S11] C. L. Kane and M. P. A. Fisher, Edge-State Transport, in *Perspectives in Quantum Hall Effects*, edited by S. D. Sarma and A. Pinczuk (John Wiley & Sons, Ltd, 1996) Chap. 4, pp. 109–159.
- [S12] M. P. A. Fisher and L. I. Glazman, Transport in a One-Dimensional Luttinger Liquid, in *Mesoscopic Electron Transport*, edited by L. L. Sohn, L. P. Kouwenhoven, and G. Schön (Springer Netherlands, 1997) pp. 331–373.
- [S13] A. M. Chang, Chiral Luttinger liquids at the fractional quantum Hall edge, *Rev. Mod. Phys.* **75**, 1449 (2003).
- [S14] L. Balents, Orthogonality Catastrophes in Carbon Nanotubes, (1999), 10.48550/arXiv.cond-mat/9906032, cond-mat/9906032.
- [S15] M. Bockrath, D. H. Cobden, J. Lu, A. G. Rinzler, R. E. Smalley, L. Balents, and P. L. McEuen, Luttinger-liquid behaviour in carbon nanotubes, *Nature (London)* **397**, 598 (1999).
- [S16] C.-H. Hsu, P. Stano, Y. Sato, S. Matsuo, S. Tarucha, and D. Loss, Charge transport of a spin-orbit-coupled Luttinger liquid, *Phys. Rev. B* **100**, 195423 (2019).
- [S17] C. L. Kane, M. P. A. Fisher, and J. Polchinski, Randomness at the edge: Theory of quantum Hall transport at filling $\nu = 2/3$, *Phys. Rev. Lett.* **72**, 4129 (1994).
- [S18] C. L. Kane and M. P. A. Fisher, Impurity scattering and transport of fractional quantum Hall edge states, *Phys. Rev. B* **51**, 13449 (1995).
- [S19] C. Chen, A. H. Castro Neto, and V. M. Pereira, Correlated states of a triangular net of coupled quantum wires: Implications for the phase diagram of marginally twisted bilayer graphene, *Phys. Rev. B* **101**, 165431 (2020).
- [S20] T. Giamarchi, *Quantum Physics in One Dimension* (Oxford University Press, New York, 2003)